MR Detection of Intracranial Calcification: A Phantom Study

Jay S. Tsuruda[1,2]
William G. Bradley[1,3]

To make a comparative analysis of calcium detection between MR and CT, anhydrous, insoluble calcium carbonate spheres varying in size from 1.5–7.0 mm were embedded in three physiologic tissue phantoms: low-protein gelatin (3 gm%), high-protein gelatin (6 gm%), and heavy mineral oil. The calcium-containing phantoms were scanned by CT and MR, using both T1- and T2-weighted sequences, with a slice thickness varying from 5–7 mm. Partial volume artifacts were determined by abutting phantoms with and without calcium and by varying the slice position to include different proportions of the calcium- and noncalcium-containing phantoms. Contrast-detail curves, expressed as a ratio of contrast to noise, were determined for varying sizes of calcification and degrees of partial voluming. As expected, the CT conspicuity of calcification (positive contrast) markedly surpasses that of MR (negative contrast). The difference was two orders of magnitude. When the calcification filled more than half the slice on MR, the conspicuity depended on the contrast of the matrix material; i.e., *increased* matrix intensity caused *increased* conspicuity. However, as the size of the calcification decreased, partial volume effects increased; i.e., *increased* matrix intensity caused *decreased* conspicuity. Conspicuity of small calcifications is independent of matrix material, since contrast and partial volume effects balance.

We conclude that CT is clearly the method of choice for identifying small foci of calcification.

As the use of MR for primary screening of CNS disease has become more common, limitations in its ability to detect calcification compared with CT have been described [1–5]. Physiologic calcification contains little MR-visible hydrogen and thus may produce no MR signal and appear as a signal void within higher-intensity parenchyma. In recent published reports of calcified intracranial lesions [4, 5], prospective identification of calcium on MR, especially fine or punctate foci, was poor compared with CT and may contribute to the reported lack of specificity with MR. Physiologic calcification can occur in tissues with a wide range of MR signal intensities such as fatty or proteinaceous matrixes. Calcification of varying size can reside partially within the imaging plane, and partial volume effects will be variable. The purpose of this study was to identify and quantify the factors that affect the detection of calcification of various sizes in different matrix materials. Contrast-to-noise ratios (CNR) were measured in phantoms evaluated by both CT and MR.

Materials and Methods

Three separate phantoms were constructed. Each contained, anhydrous, insoluble calcium carbonate spheres ranging in size from 1.5–7.0 mm, which were attached to plastic film with minute amounts of cyanoacrylate glue. This assembly was suspended across the bottom of a plastic petri dish filled to a depth of 1.5 cm with the following media: 3 gm% gelatin, 6 gm% gelatin, and heavy mineral oil. The gelatin media were prepared by modification of a protocol for biological phosphate surface-coil phantoms [6]. A second petri dish filled with the identical

Received January 26, 1987; accepted after revision May 20, 1987.

Presented at the 24th annual meeting of the American Society of Neuroradiology, San Diego, January 1986.

[1] NMR Imaging Laboratory, Huntington Medical Research Institutes, 10 Pico St., Pasadena, CA 91105. Address reprint requests to W. G. Bradley.

[2] Department of Radiology, University of California School of Medicine, San Francisco, CA 94143.

[3] Department of Radiology, Huntington Memorial Hospital, Pasadena, CA 91105.

***AJNR* 8:1049–1055, November/December 1987**
0195–6108/87/0806–1049

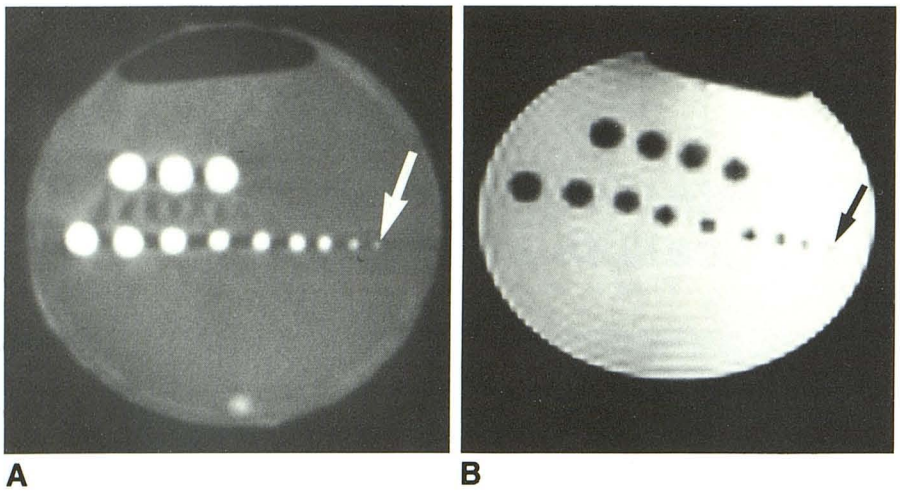

Fig. 1.—Calcium phantoms.
***A*, CT image of 6-gm% gelatin phantom.**
***B*, MR image (TR = 1.0 sec, TE = 28 msec) of 3-gm% gelatin phantom. In both instances, the smallest-diameter calcium spheres (*arrows*) can be identified.**

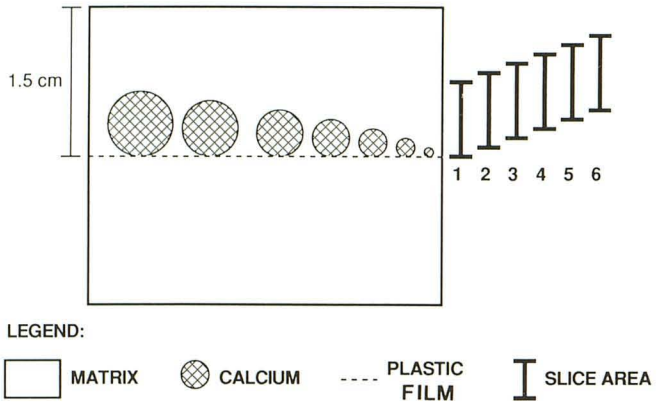

Fig. 2.—Experiment 2 (partial volume effects). Cross-sectional view of a phantom. The phantom was withdrawn after each image acquisition at 1-mm table increments starting from position 1 so that the volume covered by each slice included increasing amounts of matrix material. For each phantom, a total of 6 table increments was used.

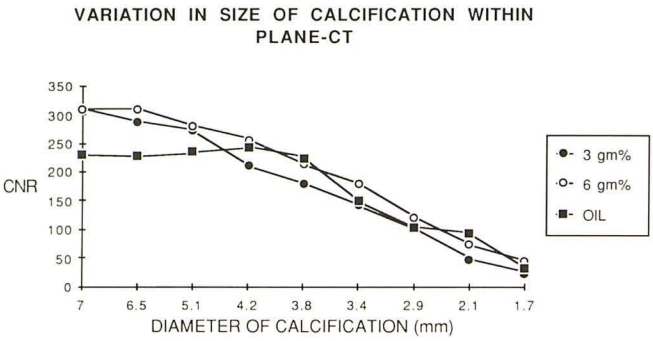

Fig. 3.—Experiment 1. CT contrast-detail curves for the three phantoms.

matrix material without the calcium spheres was applied to the opposite side of the plastic film. Care was taken to remove all air bubbles. With this method, the spheres were suspended within the center of 3 cm of matrix. The plastic film was a visible landmark that facilitated the localization and centering of the spheres within the scanner prior to imaging.

MR images were obtained with a Diasonics 0.35-T MR imager. A 128 × 128 imaging matrix was used, with a pixel size of 1.7 mm^2 and a slice thickness of 7 mm. A 15-cm double saddle coil was used. After aligning the phantoms using localizing sagittal and coronal views, all studies were obtained with a multislice, multiecho spin-echo technique with four excitations and TR = 1.0 or 2.0 sec, and TE = 28 and 56 msec.

CT images were obtained with a GE 8800 CT/T scanner with 5-mm collimation, mA = 160, kV = 120 and slow scan-speed setting.

With both scanners, the imaging sequence was performed in two parts. First, a single image was acquired in which all spheres were alligned within the selected slice (experiment 1). Representative images are shown in Figure 1. Second, multiple images were obtained as the phantom was withdrawn at 1-mm table increments up to a maximum of 6 mm. Thus, the initial image in this series was obtained with the calcification entirely within the slice. Successive images were obtained with progressively greater proportions of matrix filling the image plane in order to simulate partial volume effects (experiment 2) as shown in Figure 2.

Data were presented as a contrast-detail curve; i.e., CNR versus size of calcification. The CNR was obtained by using operator-defined regions of interest to measure both the central pixel intensity of each sphere and the background intensity within the phantom. The central pixel intensity was the maximum density reading on CT and the minimum signal intensity on MR. Background intensities were measured from identical areas within each phantom. Using previously described methods [7–9], CNR was calculated as follows:

$$CNR = \frac{|Sc - Sb|}{SDn}$$

where Sc = signal intensity of calcium, Sb = signal intensity of background, and SDn = standard deviation of the background noise. The absolute value of the ratio was used to simplify the comparison between positive contrast (i.e., calcium intensity brighter than background) with CT and negative contrast with MR. The highest background signals were found using the 6 gm% phantom on the TR 2.0 sec, TE 28 msec MR study; the lowest were the negative attenuation values found with the oil phantom using CT.

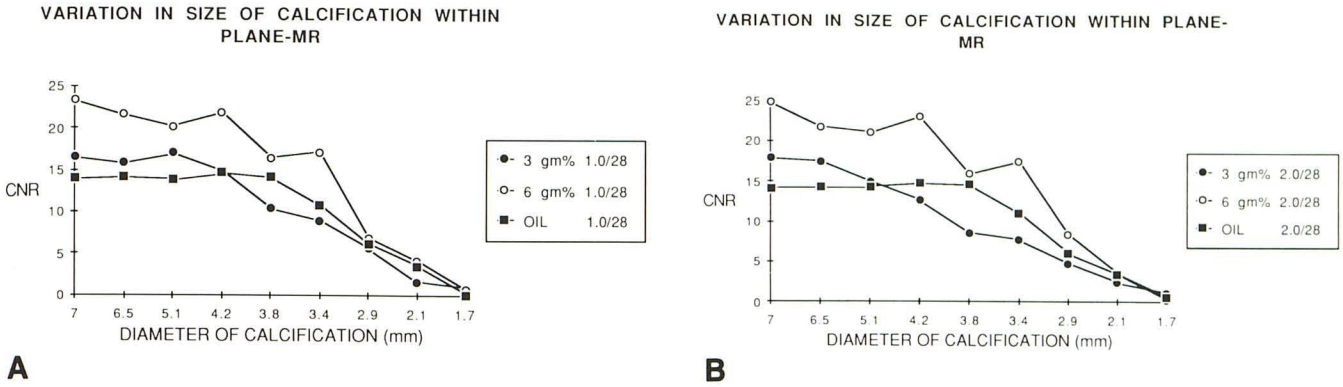

Fig. 4.—Experiment 1. MR contrast-detail curves for the three phantoms. *A*, TR 1.0 sec, TE 28 msec. *B*, TR 2.0 sec, TE 28 msec.

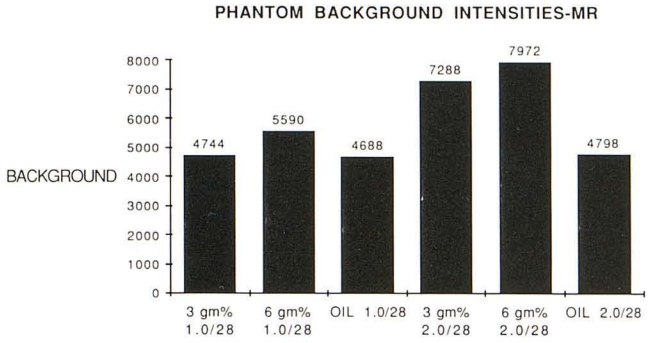

Fig. 5.—MR matrix intensities. Background intensity shown for each phantom type in arbitrary units. The TR was either 1.0 or 2.0 sec, and the TE was 28 msec in all cases.

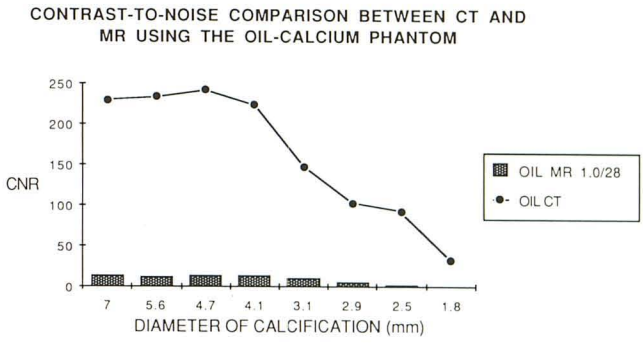

Fig. 6.—Comparison of CT and MR contrast-detail curves. With oil phantom, large differences are noted in contrast-to-noise ratios between CT and MR (TR = 1.0 sec, TE = 28 msec). Note that the minimum contrast-to-noise ratio value on CT exceeds the maximum contrast-to-noise ratio obtained by MR.

Results

Experiment 1: Variation in Size of Calcification Within the Selected Slice

The results of the experiment are expressed as a contrast-detail curve using CNR versus the diameter of the calcification in millimeters for CT (Fig. 3) and MR (Fig. 4). In Figure 3, the 7-mm calcifications showed the highest contrast to noise for both the 3- and 6-gm% phantoms. The background intensity for the 6-gm% phantom is slightly higher (avg. = 21 H) compared with the 3-gm% phantom (avg. = −1 H) with similar standard deviations. In comparison, the CNR values corresponding to the large calcifications with the oil phantom are uniformly lower. With decreasing particle size, the slope of the line and CNR values at the smallest particle size are nearly similar in all cases.

The MR results for these phantoms are shown in Figure 4. Figure 4A represents the most T1-weighted sequence (TR 1.0 sec, TE 28 msec). Compared with the CT study, the initial CNR starts at a much lower level for all three types of phantoms. With MR, the initial CNR is highest with the 6-gm% phantom, intermediate with the 3-gm% phantom, and lowest with the oil phantom. This finding parallels the measured background intensities, with 6 gm % being the highest, as noted in Figure 5. As the particle size becomes smaller, the lines converge and become nearly identical; i.e., the detectability (conspicuity) of small calcifications is independent of matrix material intensity.

Figure 4B is the contrast-detail curve from the mildly T2-weighted study (TR 2.0 sec, TE 28 msec). The CNR for large-diameter calcifications is on the same order as that found in the more T1-weighted study. Again, this parallels the background intensities shown in Figure 5. If only the background intensities are considered, the predicted CNR values should have been higher for the gelatin phantoms on the more T2-weighted study; however, the standard deviations of the backgrounds of the gelatin phantoms were also higher than in the oil phantom. (Note that the initial CNR values with the oil phantom are similar in Figures 4A and 4B, corresponding to balanced changes in Sc − Sb and SDn on the T1- and T2-weighted studies.) As seen on the T1-weighted studies, the lines are again noted to converge to similar values with decreasing particle size. Figure 6 graphically depicts the

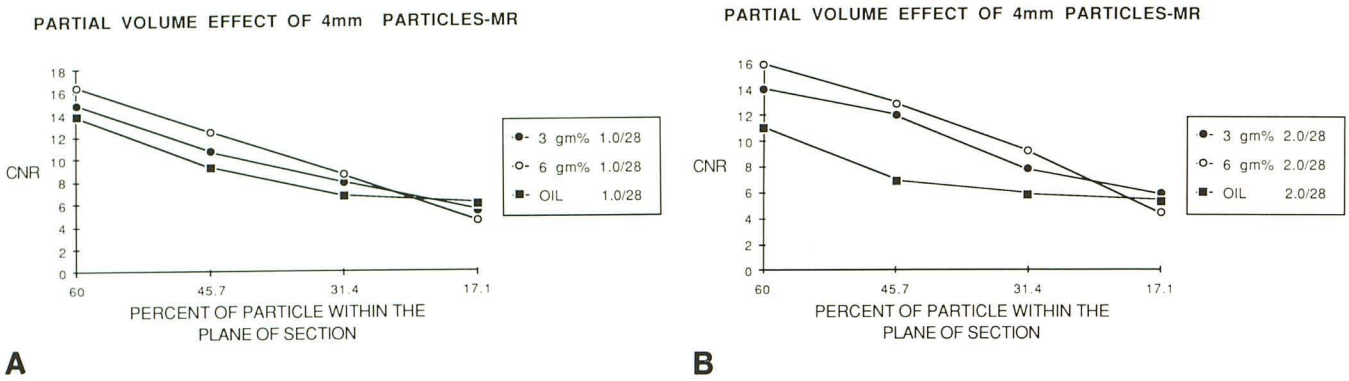

Fig. 7.—Experiment 2. Contrast-detail curves showing the effect of partial volume on 4-mm particles.
***A*, TR 1.0 sec, TE 28 msec.**
***B*, TR 2.0 sec, TE 28 msec.**

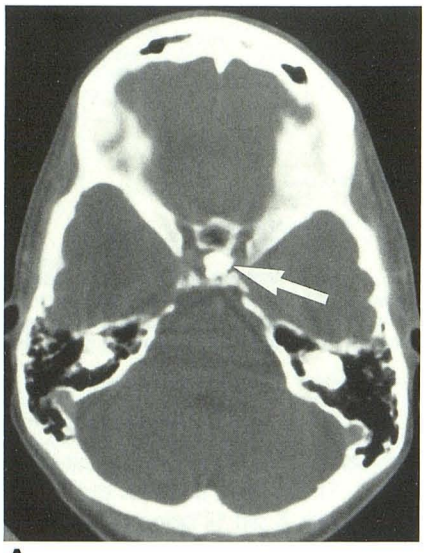

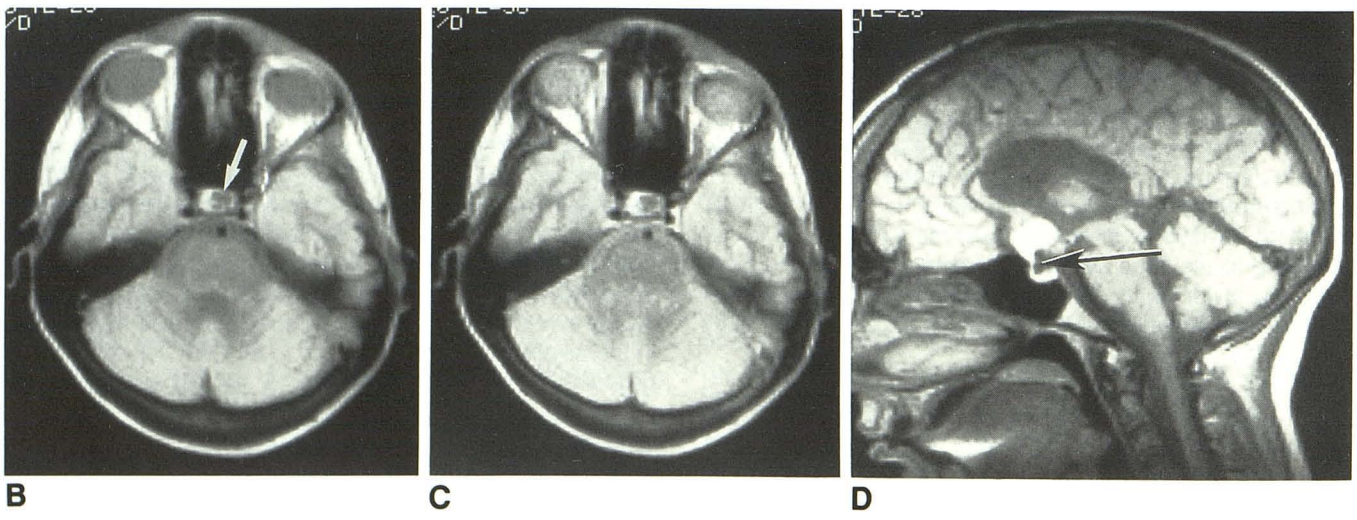

Fig. 8.—Craniopharyngioma.
***A*, Nonenhanced CT.**
***B*, TR 2.0 msec, TE 28 msec.**
***C*, TR 2.0 msec, TE 56 msec.**
***D*, TR 0.5 sec, TE 28 msec. The large calcification (*arrow*) within this craniopharyngioma was identified on both the T1- and T2-weighted images. Note that first- and second-echo images (*B* and *C*) have similar conspicuity as predicted from the phantom studies.**

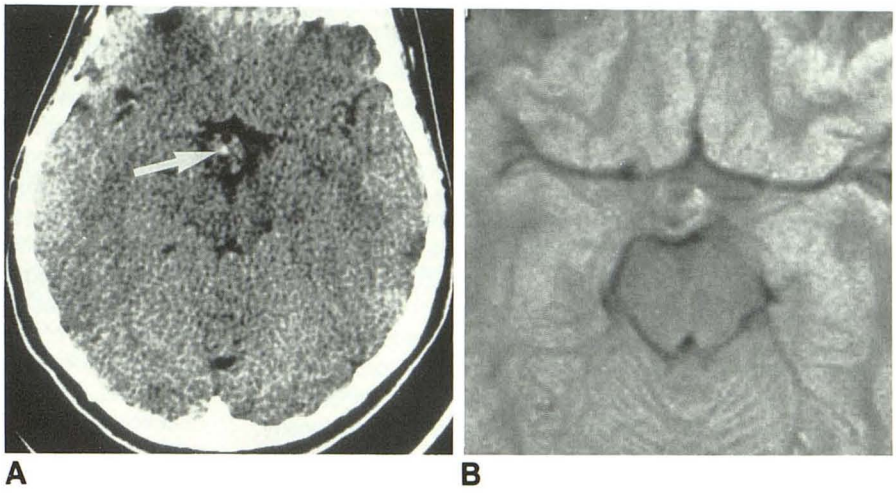

Fig. 9.—Craniopharyngioma.
***A*, Nonenhanced CT.**
***B*, TR 2.0 sec, TE 28 msec. Although readily identified on CT (*arrow*), the calcification was completely nonvisualized on MR, thus demonstrating partial volume effect. Note the two foci of low density immediately anterior and posterior to the calcific focus on CT. These can also be seen on MR as signal intensity similar to CSF and presumably representing cysts.**

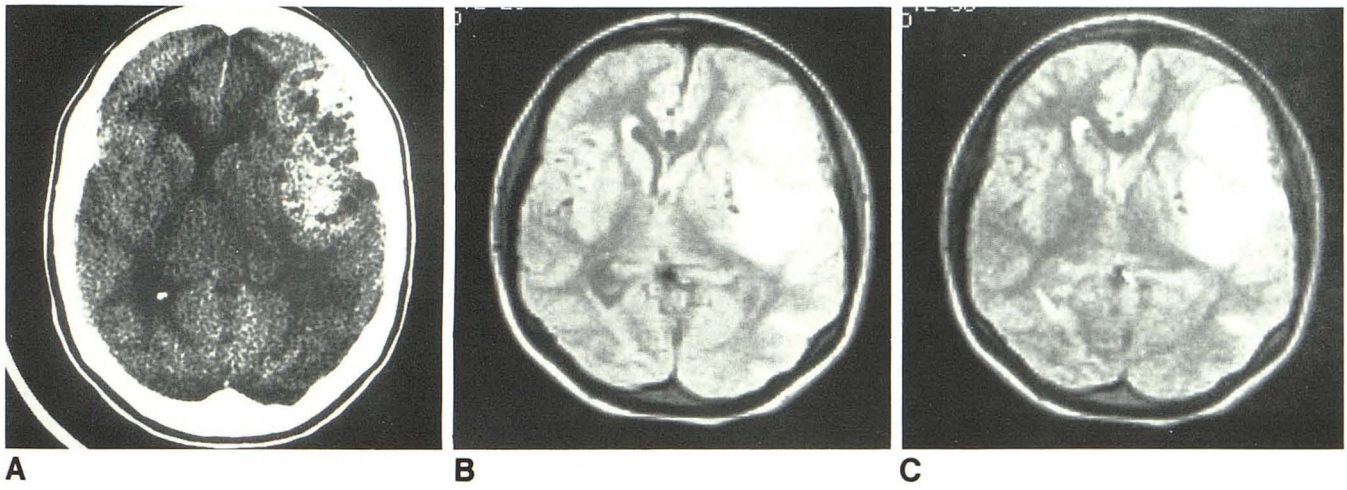

Fig. 10.—Ewing sarcoma (biopsy proved).
***A*, Nonenhanced CT.**
***B*, TR 2.0 sec, TE 28 msec.**
***C*, TR 2.0 sec, TE 56 msec. Despite showing extensive calcification on CT, poor conspicuity was noted on comparable MR studies owing to partial volume effect.**

marked differences between the observed CNR values using CT and MR.

The corresponding TE 56 msec images for both the TR 1.0 and 2.0 sec studies were also analyzed (not shown) and yielded similar results in the CNR with respect to both particle size and line slope.

Experiment 2: Partial Volume Effects

As the phantoms were gradually withdrawn from the selected slice by 1-mm intervals, it was possible to measure the CNR of each sphere with respect to the estimated percentage of filling of the $1.7^2 \times 7$ mm voxel. A representative example is seen in Figures 7A (TR = 1.0) and 7B (TR = 2.0) for 4-mm-sized spheres. Both are first-echo (TE 28 msec) images. The initial CNR demonstrates a trend similar to that with experiment 1, reflecting the differences in the background intensity. In addition, the lines for each phantom tend to converge with decreased filling of the voxel, reflecting increased partial volume effect of the high-intensity matrix material.

Clinical Examples

Figures 8 and 9 represent two different patients with calcified craniopharyngiomas. In the first case, a large sellar region calcification can be identified readily on CT. On the corresponding MR scans, both the T1- and T2-weighted images demonstrate focal areas of decreased signal intensity surrounded by higher-intensity matrix. In the second example, with much smaller calcification and therefore greater partial volume effect, decreased conspicuity is noted. Another example of partial volume of calcification is shown in Figure 10

of a pathologically proved atypical Ewing's sarcoma in a 23-year-old patient. On the CT section, lacelike calcification can be readily identified. This calcification could not be identified on the comparable MR sections.

Discussion

CT image contrast depends on the degree of attenuation of the X-ray beam. Contrast is highest when differences in attenuation are large. Calcification, by virtue of its high atomic number compared with either water or soft tissue, has a higher probability of undergoing photoelectric absorption than Compton scattering. Since photoelectric effect produces no scattered radiation, conspicuity of calcification is enhanced.

On the other hand, in the case of MR, nuclear spin density, T1, T2, and motion determine the intensity of the signal received [10]. When protons are associated with solids, T2 becomes exceedingly short, leading to a signal void on clinical studies [2, 4, 5]. Overall, MR contrast discrimination between objects is based on multiple parameters including T1, T2, proton density, and the pulsing sequences used for data acquisition. In this study, contrast discrimination was performed by comparing the intensities of the backgrounds of the phantoms and calcium spheres with the inherent noise level of the image.

There are several advantages in using this method of calculating contrast. First, the expected wide range of background intensities can be compared directly with the corresponding calcium signal. As a result, direct comparisons can be made between multiple images within the same phantom or between images acquired using either T1- or T2-weighted pulsing sequences [10], or CT. Second, division by the standard deviation of noise allows for quantification of the various factors that can affect overall image quality, including beam-hardening artifact due to calcium on CT or, on MR, to radio-frequency noise interference, losses in the receiver coil, or conduction losses within the subject [8]. Therefore, a quantitative statement about the conspicuity of calcification within the various physiologic matrixes can be made.

In experiment 1, CT demonstrated uniformly high contrast-to-noise with all three phantoms. Of interest was the lower-than-expected CNR seen with the larger particles in the oil phantom. This was thought to be due to several factors, including the negative background intensity of the oil (avg. = −171 H) causing a lower calcium intensity due to partial volume artifact and increased standard deviation of noise within the background due to streak artifact.

The experiment 1 MR data, obtained when all of the various-sized spheres were positioned within the plane of section, demonstrated several important findings. First, when the calcification filled more than half the slice volume, the conspicuity depended on the contrast between the matrix material and the signal void associated with the calcification. In other words, with a brighter background intensity, the calcification became more apparent and the conspicuity increased. This confirms the clinical observations made by Oot et al. [5].

Increasing the TR from 1.0 to 2.0 sec did not appreciably change the contrast-detail curves. This was due to the simultaneous increase of both the background intensities and the standard deviation of the noise associated with the longer repetition time. As a result, these two changes had opposite effects on the calculated CNR.

On the other hand, the differences in matrix intensity had a weaker effect on the MR calcium conspicuity when the calcium filled less than half the slice; i.e., with decreasing particle sizes of less than approximately 3 mm in diameter (experiment 1) or decreasing the amount of voxel filling (experiment 2). In both experiments, the CNR converged to the same minimum values regardless of matrix intensity. This was attributed to a greater role of partial volume effect, which minimized the contrast differences between the calcium and background intensities. This implies that as matrix intensity increases, relatively greater partial volume effect occurs; thus, conspicuity of small calcifications may be less than expected.

The second-echo images (TE 56 msec) did not provide any additional information on the conspicuity of calcification since there was little or no change in the CNR. This latter fact is a helpful finding when interpreting clinical studies, since signal void or diminution on the first-echo study may represent flowing blood [11]. The relative lack of signal change associated with calcium on the second-echo image compared with the surrounding tissues can be anticipated, whereas increased signal due to even-echo rephasing [11] may be identified if the flow is slow and laminar.

Additional causes of signal diminution on clinical MR studies—including tissue heterogeneity, such as necrosis and rapidly flowing or turbulent blood [12] within vessels—may be even more difficult to distinguish from small calcifications. Although the above experiments did not attempt to evaluate the effect of increasing background heterogeneity, it can be predicted that the standard deviation of the background "noise" would increase, thus reducing the overall CNR even further.

Although variation of the slice thickness on the MR study was not determined, conspicuity as a function of slice thickness can be predicted. From Figure 4, the contrast to noise tends to plateau toward a maximum value when the calcium sphere fills greater than 50% of the slice thickness. As an example, if a calcification of interest is 4 mm in diameter and resides totally within the slice plane, the best contrast to noise might be expected with a 4-mm slice. However, an 8-mm slice may have nearly equal conspicuity. Finally, when compared with CT, the measured CNR is two orders of magnitude higher. Therefore, CT is clearly the method of choice for identifying small foci of calcification.

ACKNOWLEDGMENTS

We are grateful for the excellent technical help given by Terry Andrues, Jay Mericle, Leslee Watson, and Jose Jiminez.

REFERENCES

1. Bradley WG, Waluch V, Yadley RA, Wycoff RR. Comparison of CT and MR in 400 patients with suspected disease of the brain and spinal cord. *Radiology* **1984**;152:695–702
2. Brant-Zawadzki M, Badami JP, Mills CM, Norman D, Newton TH. Primary

intracranial tumor imaging: a comparison of magnetic resonance and CT. *Radiology* **1984**;150:435–440
3. Lee BCP, Kneeland JB, Cahill PT, Deck MDF. MR recognition of supratentorial tumors. *AJNR* **1985**;6:871–878
4. Holland BA, Kucharcyzk W, Brant-Zawadzki M, Norman D, Haas DK, Harper PS. MR imaging of calcified intracranial lesions. *Radiology* **1985**;157:353–356
5. Oot RF, New PFJ, Pile-Spellman J, Rosen BR, Shoukimas GM, Davis KR. The detection of intracranial calcifications by MR. *AJNR* **1986**;7:801–809
6. Applications note 850125. *Biological phosphate surface coil phantom*. Fremont, CA: General Electric NMR Instruments, **1986**
7. Edelstein WA, Bottomley HR, Hart HR, Smith LS. Signal, noise, contrast in nuclear magnetic resonance (NMR) imaging. *J Compt Assist Tomogr* **1983**;7:391–401
8. Hart HR, Bottomley PA, Edelstein WA, et al. Nuclear magnetic resonance imaging: contrast-to-noise as a function of strength of magnetic field. *AJR* **1983**;141:1195–1201
9. Stark DD, Felder RC, Wittenberg J, et al. Magnetic resonance imaging of cavernous hemangioma of the liver: tissue-specific characterization. *AJR* **1985**;145:213–222
10. Wehrli FW, MacFall JR, Shutts D, Breger R, Herfkens RJ. Mechanisms of contrast in NMR imaging. *J Compt Assist Tomogr* **1984**;8:369–380
11. Waluch V, Bradley WG. NMR even echo rephasing in slow laminar flow. *J Compt Assist Tomogr* **1984**;8:594–598
12. Bradley WG, Waluch V. Blood flow: magnetic resonance, imaging. *Radiology* **1985**;154:443–450